Remote sensing analysis of spatiotemporal habitat evolution in the water-land ecotone of a typical large river-connected lake

Yifan Xu*, Tengfei Hu, Hao Lu

Laboratory of Water Disaster Prevention, Nanjing Hydraulic Research Institute, 210029 Nanjing, China

Abstract. The water-land ecotone of Dongting Lake is one of the most sensitive zones to river-lake interactions and one of the most complex areas in terms of coupled ecological processes. Using the Google Earth Engine platform and six phases of Landsat and Sentinel-2 images acquired during 1993–2023, this study constructed a multi-source feature set and applied a random forest classifier to identify habitats in the Dongting Lake water-land ecotone. The spatiotemporal evolution of habitats was analyzed for the whole lake and for the eastern, southern, and western sub-lakes over the past 30 years. The results show that the water area in the dry season decreased from 775.36 km² in 1993 to 554.41 km² in 2023, a reduction of 28.5%. Grass shoals exhibited a pronounced V-shaped trajectory, emergent vegetation showed an inverted V-shaped trajectory, and poplar forest underwent three stages of expansion, decline, and stabilization. Marked spatial differences were found among the three sub-lakes. These results provide a data basis for wetland conservation, ecological restoration, and river-lake regulation in Dongting Lake.

1 Introduction

Large river-connected lakes in the middle and lower reaches of the Yangtze River constitute one of the most dynamic composite ecosystems in terms of river-lake interactions and play important roles in flood regulation and storage, freshwater supply, water purification, habitat maintenance, and biogeochemical cycling [1-3]. Dongting Lake, as a typical through-flow river-connected lake, is jointly controlled by backwater effects from the Yangtze River and inflow from its tributary basin. It is characterized by pronounced alternations between high-water and low-water periods, and its extensive water-land ecotone is the most sensitive area where lacustrine ecological processes and hydrological processes interact. It also plays a key role in maintaining the health of the wetland ecosystem [4-6].

In recent decades, the combined effects of upstream reservoir regulation, climate change, variations in basin inflow, lake-basin geomorphic evolution, and human activities have substantially altered the hydrosedimentary processes and hydrological rhythm of Dongting Lake, thereby driving continuous adjustments in the area of the water-land ecotone, vegetation types, and shoal patterns [7-10]. These changes are directly related to wetland ecosystem stability, the quality of migratory bird habitats, and the ecological security of the lake region. Therefore, research on the spatiotemporal evolution of habitats in the Dongting Lake water-land ecotone is of both scientific and practical significance.

Remote sensing has become an important tool for habitat monitoring in lake wetlands because of its broad spatial coverage, strong capability for dynamic and continuous observation, and suitability for long-term comparative analysis [11-13]. Long-term Landsat archives have been widely used to reconstruct wetland extent and vegetation dynamics over decadal timescales, providing a consistent basis for identifying hydrological and ecological transitions in wetland systems [14]. With the increasing availability of Sentinel-1/2 imagery, recent studies have further demonstrated that the integration of optical, radar, topographic, and phenological features can improve the discrimination of complex wetland classes, particularly in areas with frequent inundation, mixed vegetation communities, and high intra-class spectral variability [15,16]. Google Earth Engine and machine-learning algorithms, such as random forest and decision-tree-based classifiers, have also enabled efficient wetland mapping over large spatial domains and long observation periods [17]. For Dongting Lake, previous studies have integrated Sentinel-1/2 and DEM data with ensemble classifiers on the Google Earth Engine platform to map wetland vegetation distribution and analyze long-term vegetation dynamics, demonstrating the potential of multi-source remote sensing for characterizing wetland landscape heterogeneity [18].Existing studies have mainly focused on a single period or a local area, while continuous comparisons of habitat patterns at the whole-lake scale during the dry season remain insufficient for Dongting Lake. Accordingly, this study employs the Google Earth Engine (GEE) platform, integrates multi-source Landsat and Sentinel-2 imagery, and applies a random forest classifier to six dry-season images acquired between 1993 and 2023, with the aim of systematically revealing the habitat evolution of the Dongting Lake water-land ecotone and the differences among sub-lakes.

*Corresponding author: xuyf@nhri.cn

2 Study area and data

2.1 Study area

Dongting Lake is located on the southern bank of the middle reaches of the Yangtze River in northern Hunan Province, China, and is a typical through-flow river-connected lake (Fig. 1). Lake water levels are jointly controlled by the hydrological regime of the Yangtze River and inflow from the catchment, producing a marked seasonal rhythm of "flooding as lake, recession as shoal": the water surface expands during the high-water season, whereas shoals are widely exposed during the dry season. According to the natural geographical pattern and the conventional regional division, Dongting Lake can be divided into eastern, southern, and western sub-lakes. These sub-lakes differ significantly in their connectivity with the Yangtze River, the regulation imposed by inflowing rivers, lake-basin morphology, and wetland vegetation distribution, thereby providing a basis for analyzing spatial habitat differentiation.

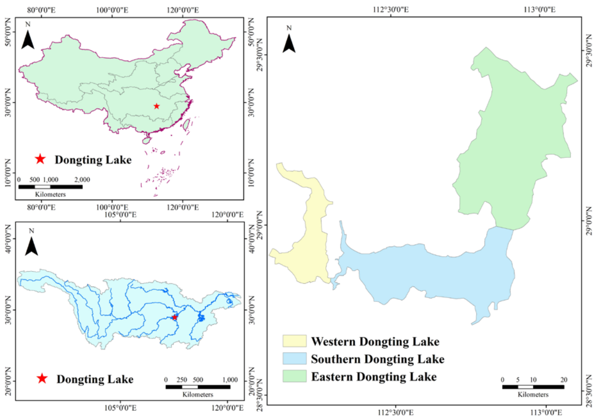

Fig. 1. Study area.

2.2 Remote sensing data

All remote sensing data used in this study were obtained through the GEE platform [19], including Sentinel-2 MSI L2A data, Landsat-5 TM data, Landsat-8 OLI data, and SRTM 30 m digital elevation data (USGS/SRTMGL1_003). Because most shoals in Dongting Lake are exposed during the winter dry season and reeds enter the senescence and harvest period, they can be more readily distinguished from Carex marshes in remote sensing images. In addition, vegetation is at the end of the growing season during this period, and interannual fluctuations are relatively small, which improves comparability among years. Therefore, the classification images were consistently selected from December to January of the following year. Six dry-season image phases were used: Landsat-5 images for 1993, 1999, and 2008; a Landsat-8 image for 2014; and Sentinel-2 images for 2017 and 2023.

3 Methods

3.1 Remote sensing identification of the Dongting Lake water-land ecotone

Based on optical remote sensing imagery, a random forest (RF) algorithm [20] was used to identify and interpret habitats in the Dongting Lake water-land ecotone during the winter dry season. The habitats were classified into five types: water (including open lake water and river channels), poplar forest (mainly plantations of Euro-American poplar), grass shoal (mainly Carex marsh), emergent vegetation (tall emergent plants such as reeds, including both pre-harvest and post-harvest phenological states merged into one class), and mudflat (bare or sparsely covered exposed shoals). RF is a supervised classification method based on an ensemble of decision trees. It integrates multidimensional feature variables for classification and is characterized by high accuracy, strong stability, and high robustness to noise, making it particularly suitable for wetland image classification in areas with complex land-cover types and highly dynamic water-land boundaries. For model training and validation, the interpreted sample points were randomly divided into training and validation datasets at a ratio of 7:3. The number of decision trees was set to 100, which was considered sufficient to ensure classification stability while maintaining computational efficiency.

Feature variables were selected according to the spectral and ecological characteristics of the main habitat types in Dongting Lake water-land ecotone. According to the characteristics of Landsat-5/8 and Sentinel-2 imagery, separate sets of classification variables were constructed, including spectral bands, major spectral indices, and terrain variables derived from SRTM. The spectral indices included the normalized difference vegetation index (NDVI), normalized difference water index (NDWI), bare soil index (BSI), index-based built-up index (IBI), modified normalized difference water index (MNDWI), green atmospherically resistant index (GARI), visible atmospherically resistant index (VARI), modified soil-adjusted vegetation index (MSAVI), and plant senescence reflectance index (PSRI). To further improve classification accuracy, terrain variables, including elevation, slope, and aspect, were introduced in addition to spectral features (Table 1).

Table 1. Feature variables used for random forest classification.

Feature type	Number of variables	Specific variables
Landsat-5 TM spectral bands	6	B1, B2, B3, B4, B5, B7
Landsat-8 OLI spectral bands	6	B2, B3, B4, B5, B6, B7
Landsat spectral indices	6	NDVI, NDWI, BSI, IBI, MNDWI, GARI
Sentinel-2 MSI spectral bands	9	B2, B3, B4, B5, B6, B7, B8, B8A, B11
Sentinel-2 MSI spectral indices	9	NDVI, NDWI, BSI, IBI, MNDWI, GARI, VARI, MSAVI, PSRI
Terrain variables	3	elevation, slope, aspect

3.2 Statistical analysis and accuracy assessment

Thirty percent of the sample points were used as the validation dataset, and classification accuracy was evaluated using the confusion matrix and the two derived statistics of overall accuracy (OA) and the Kappa coefficient. OA represents the proportion of correctly classified pixels in the validation dataset and is a widely used indicator of overall classification performance. Because OA can be biased when class proportions differ markedly, the Kappa coefficient is also reported to account for agreement expected by chance; values larger than 0.8 indicate almost perfect agreement. In Eqs. (1) and (2), q denotes the number of classes, n_{ii} denotes the diagonal elements of the confusion matrix, n_{i+} and n_{+i} denote the row and column totals of the confusion matrix, respectively, and n denotes the total number of pixels used in the accuracy assessment.

$$\mathrm{OA} = \frac{\sum_{i=1}^{q} n_{ii}}{n} \times 100\% \tag{1}$$

$$\mathrm{Kappa} = \frac{n\sum_{i=1}^{q} n_{ii} - \sum_{i=1}^{q} n_{i+}n_{+i}}{n^2 - \sum_{i=1}^{q} n_{i+}n_{+i}} \times 100\% \tag{2}$$

4 Results

4.1 Classification accuracy assessment

The classification accuracy of all interpreted images was high (Table 2). OA ranged from 88.66% to 94.48%, and the Kappa coefficient ranged from 0.8599 to 0.9303. These results indicate that the random forest classification based on multi-source imagery, spectral indices, and terrain variables can effectively distinguish the main habitat types in Dongting Lake during the dry season and is suitable for long-term analysis of habitat evolution.

Table 2. Classification accuracy of the interpreted images.

Image period	OA	Kappa
Dec. 1993 (Landsat-5)	89.38%	0.8661
Dec. 1999 (Landsat-5)	94.48%	0.9303
Dec. 2008 (Landsat-5)	88.66%	0.8599
Jan. 2014 (Landsat-8)	91.59%	0.8959
Dec. 2017 (Sentinel-2)	91.64%	0.8977
Dec. 2023 (Sentinel-2)	93.09%	0.9128

4.2 Evolution of habitat areas for the whole lake

During the past 30 years, habitat types in Dongting Lake changed substantially (Fig. 2). In general, the water area continuously decreased, grass shoals and emergent vegetation exhibited V-shaped and inverted V-shaped trajectories, respectively, poplar forest first expanded and then receded before stabilizing, and mudflat area fluctuated strongly.

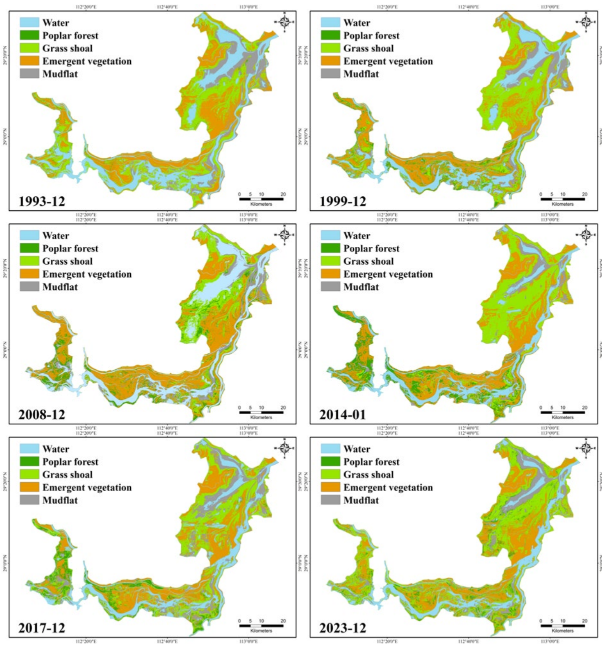

Fig. 2. Spatiotemporal distribution of habitat types in Dongting Lake during the six dry-season periods.

The water area decreased from 775.36 km² in December 1993 to 554.41 km² in December 2023, representing a net loss of 220.95 km² (a 28.5% reduction). Grass shoal area declined from 812.80 km² to 499.16 km² by December 2008 and then recovered continuously, reaching 906.65 km² in December 2023. In contrast, emergent vegetation increased from 845.77 km² to 1027.31 km² in December 2008 and then gradually declined to 861.58 km² in December 2023. Both classes showed a turning point around 2008, suggesting a clear substitution between the two habitats. Poplar forest changed most dramatically, increasing from 49.77 km² in December 1993 to a peak of 317.04 km² in January 2014, followed by a decline and stabilization at approximately 210 km² after 2017. Mudflat area fluctuated between 260.42 km² and 518.19 km² and generally varied inversely with water area, reflecting the process by which lower dry-season water levels promote shoal exposure and mudflat expansion (Table 3).

4.3 Spatial differences in habitat evolution among the sub-lakes

In December 1993, emergent vegetation was the dominant habitat in Eastern Dongting Lake, with an area of 457.25 km², followed by grass shoals. By December 2008, emergent vegetation was still dominant. However, by December 2017, grass shoal area had increased to 493.75 km² and exceeded emergent vegetation, and it further increased to 531.31 km² in December 2023. Over the study period, grass shoals in Eastern Dongting Lake increased by 92.97 km², whereas emergent vegetation decreased by 19.04 km², indicating a shift from an emergent-vegetation-dominated pattern to a grass-shoal-dominated pattern (Fig. 3b).

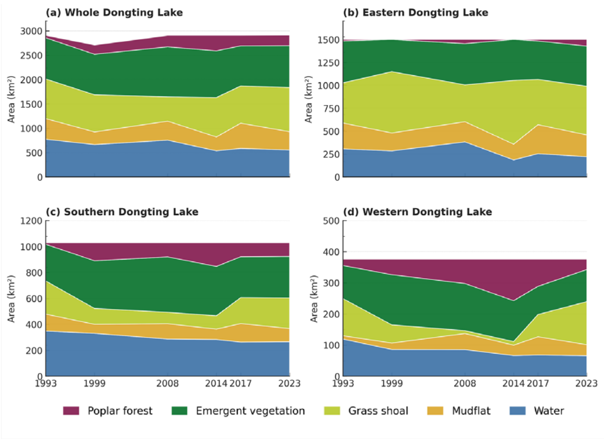

Fig. 3. Spatiotemporal habitat evolution in the Dongting Lake sub-lakes.

Emergent vegetation remained dominant in Southern Dongting Lake throughout the study period, although marked fluctuations occurred. In December 2008, emergent vegetation reached its maximum area of 426.45 km², whereas grass shoals decreased to 87.92 km², showing a pronounced seesaw relationship between the two habitat types. Thereafter, emergent vegetation declined and grass shoals recovered. By December 2023, the two areas were 319.58 km² and 235.89 km², respectively, both close to their levels in December 1993, indicating frequent interannual transitions between the two habitat types in Southern Dongting Lake (Fig. 3c).

Western Dongting Lake showed the most intense habitat fluctuations. Over the past 30 years, it experienced a succession from grass-shoal dominance to emergent-vegetation dominance and then back to grass-shoal dominance. Grass shoals were dominant in December 1993; emergent vegetation increased to 151.16 km² in December 2008, accompanied by marked expansion of poplar forest; the areas of emergent vegetation and poplar forest became comparable in December 2017; and grass shoals recovered to 138.21 km² in December 2023 and again became the dominant type. Western Dongting Lake therefore appears to be more sensitive to the combined influences of hydrological change and human disturbance (Fig. 3d).

Table 3. Evolution of habitat areas in Dongting Lake (km²).

Habitat type	1993-12	1999-12	2008-12	2014-01	2017-12	2023-12
Water	775.36	664.92	756.28	537.07	586.64	554.41
Poplar forest	49.77	190.04	233.90	317.04	213.00	211.94
Grass shoal	812.80	762.80	499.16	809.75	765.63	906.65
Emergent vegetation	845.77	832.40	1027.31	958.15	823.85	861.58
Mudflat	423.59	260.42	390.63	285.27	518.19	376.19

5 Discussion

The winter water area of Dongting Lake decreased overall during the study period, with a particularly pronounced contraction between 2008 and 2014. Hydrological data show [21] that after the initial impoundment of the Three Gorges Reservoir in 2003, the mean water level of Eastern Dongting Lake during the recession period decreased by approximately 1.05 m compared with the pre-impoundment period, and the maximum water level in October decreased by as much as 3.67 m. The backwater effect of the Yangtze River on Dongting Lake was therefore significantly weakened, leading to the shrinkage of lake water and the earlier and broader exposure of shoals during the dry season [22].

Poplar forest expanded rapidly from 1993 to 2014 and then declined markedly thereafter. This temporal pattern corresponds closely to the expansion of poplar plantations on lake shoals and the subsequent implementation of the "returning forest to wetland" ecological restoration program. At the same time, the opposite trajectories of grass shoals and emergent vegetation around 2008 suggest that different vegetation types occupy distinct niches along elevation gradients and inundation-duration gradients. Water-level fluctuations, exposure duration of shoals, and human disturbance jointly shaped the evolution of habitat structure.

Several uncertainties should be acknowledged. First, differences in spatial resolution, band configurations, and acquisition conditions among multi-source images may affect long-term comparability. Second, the interpretation of driving mechanisms in this study is primarily based on the correspondence between remotely sensed patterns and known hydrological events or ecological engineering interventions. Robust causal inference still requires further verification using water-level series, sediment processes, and field observations.

6 Conclusions

(1) From 1993 to 2023, the winter habitats in the Dongting Lake water-land ecotone underwent substantial adjustment. Water area decreased by 28.5% overall; grass shoals first decreased and then increased; emergent vegetation first increased and then decreased; poplar forest experienced three stages of expansion, decline, and stabilization; and mudflat area fluctuated markedly.

(2) Marked differences were observed among the three sub-lakes. Eastern Dongting Lake shifted from an emergent-vegetation-dominated pattern to a grass-shoal-dominated pattern; emergent vegetation remained dominant in Southern Dongting Lake but fluctuated considerably among years; and Western Dongting Lake was the most sensitive to hydrological changes and human disturbance, showing the most frequent shifts in dominant habitat type.

(3) The evolution of habitats in Dongting Lake corresponded closely in time with changes in river-lake hydrological processes and the implementation of ecological engineering measures. Long-term remote sensing monitoring can effectively reveal habitat-pattern

evolution and engineering responses, thereby providing long-term consistent data support for wetland conservation, ecological restoration, and river-lake regulation.

Acknowledgments

Funding: This research was funded by the National Key Research and Development Program of China (No.2023YFC3209003).

References

1. Y. Huang, X. Chen, Y. Zhuo, L. Zhu, *Water* **17**, 2337 (2025). DOI: 10.3390/w17152337
2. J. Qiu, S. Yuan, H. Tang, Q. Zhang, C. Wolter, V. Nikora, *Water Resources Research* **60**, e2024WR037495 (2024). DOI: 10.1029/2024WR037495
3. S. Wang, S. Wu, Y. Dong, X. Li, Y. Wang, Y. Li, Y. Zhu, J. Deng, X. Zhuang, *Communications Earth & Environment* **5**, 784 (2024). DOI: 10.1038/s43247-024-01912-8
4. J.T. Li, L. Chen, C.L. Wu, M. Li, D.D. Yan, S.Y. Xie, Z.Q. Luan, *Ecohydrology & Hydrobiology* **24**, 920–930 (2024). DOI: 10.1016/j.ecohyd.2023.08.012
5. F. Deng, X.L. Wang, X.B. Cai, E.H. Li, L.Z. Jiang, H. Li, R.R. Yan, *Ecohydrology* **7**, 717–726 (2014). DOI: 10.1002/eco.1393
6. H.H. Peng, H.N. Xia, Q. Shi, H. Chen, N. Chu, J. Liang, et al., *Ecological Indicators* **142**, 109283 (2022). DOI: 10.1016/j.ecolind.2022.109283
7. X.J. Lai, H. Zou, J.H. Jiang, et al., *Scientific Reports* **15**, 50 (2025). DOI: 10.1038/s41598-024-83751-3
8. X.Y. Yang, S.H. Zhang, C.H. Tang, C.S. Wu, Y.X. Ge, *Journal of Hydrology* **646**, 132302 (2025). DOI: 10.1016/j.jhydrol.2024.132302
9. L. Xing, L. Chi, S. Han, J. Wu, J. Zhang, C. Jiao, X. Zhou, *International Journal of Environmental Research and Public Health* **19**, 14180 (2022). DOI: 10.3390/ijerph192114180
10. Y. Cai, S. Liu, H. Lin, *Applied Sciences* **10**, 4209 (2020). DOI: 10.3390/app10124209
11. M. Mahdianpari, B. Salehi, M. Rezaee, F. Mohammadimanesh, Y. Zhang, *Remote Sensing* **10**, 1119 (2018). DOI: 10.3390/rs10071119
12. X. Zhang, T. Wang, X. Han, *Frontiers in Remote Sensing* **6**, 1569617 (2025). DOI: 10.3389/frsen.2025.1569617
13. Y. Deng, W. Jiang, Z. Ling, X. Wang, K. Peng, Z. Li, *International Journal of Digital Earth* **16**, 3199–3221 (2023). DOI: 10.1080/17538947.2023.2241428
14. Q. Demarquet, S. Rapinel, S. Dufour, L. Hubert-Moy, *Remote Sensing* **15**, 820 (2023). DOI: 10.3390/rs15030820
15. M. Hao, W. Feng, W. Bao, X. Zhang, X. Ma, W. Wang, *Applied Computing and Geosciences* **28**, 100294 (2025). DOI: 10.1016/j.acags.2025.100294
16. H. Yu, S. Li, Z. Liang, S. Xu, X. Yang, X. Li, *Sensors* **24**, 6664 (2024). DOI: 10.3390/s24206664
17. H. Jafarzadeh, M. Mahdianpari, E.W. Gill, F. Mohammadimanesh, *Sensors* **24**, 1651 (2024). DOI: 10.3390/s24051651
18. X. Long, X. Li, H. Lin, M. Zhang, *International Journal of Applied Earth Observation and Geoinformation* **102**, 102453 (2021). DOI: 10.1016/j.jag.2021.102453
19. N. Gorelick, M. Hancher, M. Dixon, S. Ilyushchenko, D. Thau, R. Moore, *Remote Sensing of Environment* **202**, 18–27 (2017). DOI: 10.1016/j.rse.2017.06.031
20. L. Breiman, *Machine Learning* **45**, 5–32 (2001). DOI: 10.1023/A:1010933404324
21. X.J. Lai, Q.H. Liang, J.H. Jiang, Q. Huang, *Water Resources Management* **28**, 5111–5124 (2014). DOI: 10.1007/s11269-014-0797-6
22. C. Hu, C. Fang, W. Cao, *International Journal of Sediment Research* **30**, 256–262 (2015). DOI: 10.1016/j.ijsrc.2014.05.001